Obrabotka metallov (tekhnologiya, oborudovanie, instrumenty) = Metal Working and Material Science. 2024 vol. 26 no. 2 pp. 186–198
ISSN: 1994-6309 (print) / 2541-819X (online)
DOI: 10.17212/1994-6309-2024-26.2-186-198

NSTU NETI

Obrabotka metallov - Metal Working and Material Science

Journal homepage: http://journals.nstu.ru/obrabotka_metallov

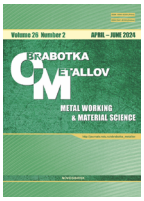

The influence of technological parameters of the laser engineered net shaping process on the quality of the formed object from titanium alloy VT23

Ksenia Bazaleeva [1, a, *], ***Daria Safarova*** [1, b], ***Yulia Ponkratova*** [1, c], ***Maxim Lugovoi*** [1, d], ***Elena Tsvetkova*** [1, e], ***Andrei Alekseev*** [1, f], ***Mark Zhelezni*** [1, j], ***Ivan Logachev*** [2, h], ***Fedor Baskov*** [2, i]

[1] Peoples' Friendship University of Russia named after Patrice Lumumba, 6 Miklukho-Maklaya st., Moscow, 117198, Russian Federation
[2] The National University of Science and Technology MISIS, 4 Leninskiy Pr., Moscow, 119049, Russian Federation

[a] https://orcid.org/0000-0002-6205-3154, bazaleeva-ko@rudn.ru; [b] https://orcid.org/0000-0002-2811-8292, safarova_de@pfur.ru;
[c] https://orcid.org/0009-0000-1094-3529, ponkratova_yuyu@rudn.ru; [d] https://orcid.org/0009-0007-7160-7802, www111www6376@gmail.com;
[e] https://orcid.org/0009-0002-8462-1818, tsvetkova-ev@rudn.ru; [f] https://orcid.org/0009-0008-7394-6370, alexeev-anvs@rudn.ru;
[j] https://orcid.org/0000-0003-3821-6790, markiron@mail.ru; [h] https://orcid.org/0000-0002-8216-1451, logachev.ia@misis.ru;
[i] https://orcid.org/0000-0001-6238-4378, baskov.fa@misis.ru

ARTICLE INFO

Article history:
Received: 25 January 2024
Revised: 19 February 2024
Accepted: 20 March 2024
Available online: 15 June 2024

Keywords:
Laser engineered net shaping
Titanium alloys
Technological parameters
Phase-structural state

ABSTRACT

Introduction. Laser engineered net shaping (*LENS*) or Direct metal deposition (*DMD*) is considered as a promising method for manufacturing products of complex configurations from titanium-based alloys, as it allows minimizing the use of machining and loss of material to waste. Currently, neither the *LENS* technological process of titanium alloy *VT23* has not been developed, nor the structural features of the alloy after *LENS* have not been studied, which will make it possible to determine the scope of application of the material after *LENS*. **The purpose of this study** is to determine optimal modes of the *LENS* process for manufacturing of quality parts from titanium alloy *VT23*. **Methodology.** The alloy specimens obtained with laser power 700÷1300 W in increments of 100 W and scanning speed 600÷1,000 mm/min in increments of 200 mm/min and distance between adjacent laser tracks 0.5–0.9***L*** (***L*** — track width) in increments of 0.2***L*** were analyzed in the study. The elemental composition of the powder material was studied by X-ray fluorescence analysis and reducing combustion in a gas analyzer, the structure of the objects obtained by *LENS* was analyzed by metallographic and X-ray phase analysis methods as well as microhardness was determined. **Results and discussion.** It is established that high-quality objects without cracks, with low porosity can be synthesized from *VT23* alloy by *LENS* method using the following modes: laser power 700÷1100 W, scanning speed 800–1,000 mm/min, track spacing 0.5–0.7 of the individual track width ***L***. It is shown that after all investigated *LENS* modes, the *VT23* alloy had a dispersed (α+β) structure of the *"basket weave"* type. It is revealed that regardless of *LENS* mode the amount of β-phase in the alloy structure is about 30 %. It is shown that the microhardness of the deposited material does not depend on *LENS* modes and is 460 HV.

For citation: Bazaleeva K.O., Safarova D.E., Ponkratova Yu.Yu., Lugovoi M.E., Tsvetkova E.V., Alekseev A.V., Zhelezni M.V., Logachev I.A., Baskov F.A. The influence of technological parameters of the laser engineered net shaping process on the quality of the formed object from titanium alloy VT23. *Obrabotka metallov (tekhnologiya, oborudovanie, instrumenty) = Metal Working and Material Science*, 2024, vol. 26, no. 2, pp. 186–198. DOI: 10.17212/1994-6309-2024-26.2-186-198. (In Russian).

Introduction

Titanium alloys are known for its high specific strength, corrosion resistance, and crack resistance and found applications in various industrial sectors, including aerospace [1]. Since many components of aircraft have a complex configurations, laser engineered net shaping (*LENS*) is considered as a promising technology for its production [2–5]. Another reason for utilizing *LENS* technology in manufacturing parts from titanium alloys is that these materials are difficult to process mechanically due to its high strength

*** Corresponding author**
Bazaleeva Ksenia O., Ph.D. (Engineering)
Peoples' Friendship University of Russia named after Patrice Lumumba,
6 Miklukho-Maklaya st.,
117198, Moscow, Russian Federation
Tel.: +7 905 760-12-32, **e-mail:** bazaleeva-ko@rudn.ru

and low thermal conductivity, while *LENS* allows the formation of complex-profiled parts with minimal mechanical processing. Moreover, diminishing mechanical processing helps reduce the amount of expensive alloy waste.

It is known that the quality of the objects manufactured by *LENS* depends on its technological parameters. Quality in this case implies the absence of macrodefects like cracks and pores that can form during laser remelting of the powder material. In [6–13] authors optimize the *LENS* technological parameters for manufacturing parts from titanium alloys by varying laser power, scanning speed, powder feed rate, laser spot diameter, distance between laser tracks and laser operating mode (pulse/continuous) [5]. However, the practical application of modes developed by other researchers is mainly hindered by two reasons. The first reason is that most researches have been conducted on the titanium alloy *Ti-6Al-4V* [4–9] and significantly less studies have been devoted to the development of *LENS* technology for titanium alloys of different compositions (*Ti-Al-Sn-Zr-Mo* [10], *Ti-Al-Sn-Zr-Mo-Cr* [11], *Ti-Al-Mo-Zr-Si* [12]), and there are almost no studies on *LENS* of the *Ti-5Al-4V-2.5Mo-1Cr-0.7Fe-0.1Si* alloy (*VT23*). However, it is known that changes in the physical properties of the alloy affect the powder material remelting processes, and the alloy composition have to be taken into account. Moreover, *LENS* is a multi-parameter process, while most papers only provide values for basic parameters. Thermal conditions of powder remelting significantly depend on the working setup, the initial state of the powder material and even slight changes in re-melting conditions can result in shift of the optimal parameter range. Thus, developing modes of manufacturing high-quality objects of a given composition is an integral part of *LENS* technology.

The purpose of this work was to develop *LENS* modes on the *InssTek MX-Grande* printer for the formation of high-quality products from a titanium alloy (*VT23*). To achieve this goal, the following tasks were solved during the research:

– determination of intervals of the *LENS* technological parameters (laser radiation power, scanning speed and distance between laser tracks), which make it possible to form a structure without cracks, with minimal porosity and surface roughness, with penetration into the lower layer less than 40 %;

– metallographic study of the structure formed in the alloy during *LENS*;

– determination of the phase composition of the alloy after *LENS*;

– study of the influence of the *LENS* technological parameters on the microhardness of the obtained material.

Methods

The objects of the study were specimens manufactured by *LENS* from titanium alloy *VT23*. X-ray fluorescence spectral analysis was used to assess the elemental composition of the initial titanium powder, and the concentrations of gas impurities in the powder were determined by the reduction burning method (Table 1). The chemical composition of the *VT23* powder, including the concentrations of gas impurities, corresponded to *OST 1-90013-81* [14]. The dispersion of the powder ranged from 40 to 100 μm. The phase composition of the initial powder material was determined by X-ray diffraction method and consisted of a α-*Ti* solid solution with a cubic crystal lattice and titanium oxide TiO_2 (rutile) phase with a tetragonal crystal lattice while β phase was not detected (Figure 1). The presence of the TiO_2 phase in the diffraction pattern is likely associated with a high proportion of the surface oxide layer in the irradiated volume of a dispersed (less than 100 μm) powder material during X-ray analysis.

LENS process was carried out on the *InssTek MX-Grande* laser system in an *Ar* protective atmosphere, and the *LENS* modes are provided in Table 2.

The selection of *LENS* modes that allow forming parts of satisfactory quality was carried out in several steps. In the first step, the selection is based on the geometric parameters of the cross-section of a single laser track. In the second step, the characteristics of monolayers, i.e., objects with a height of one deposited layer, are considered, and in the final step, the quality of the volumetric specimen is analyzed.

Table 1

Chemical composition of the experimental powder

Mass fraction of chemical elements, %									
Ti	*Al*	*V*	*Mo*	*Cr*	*Fe*	*O*	*H*	*N*	*C*
bal.	4.8	4.5	2.6	1.2	0.4	0.12	0.004	0.018	0.03

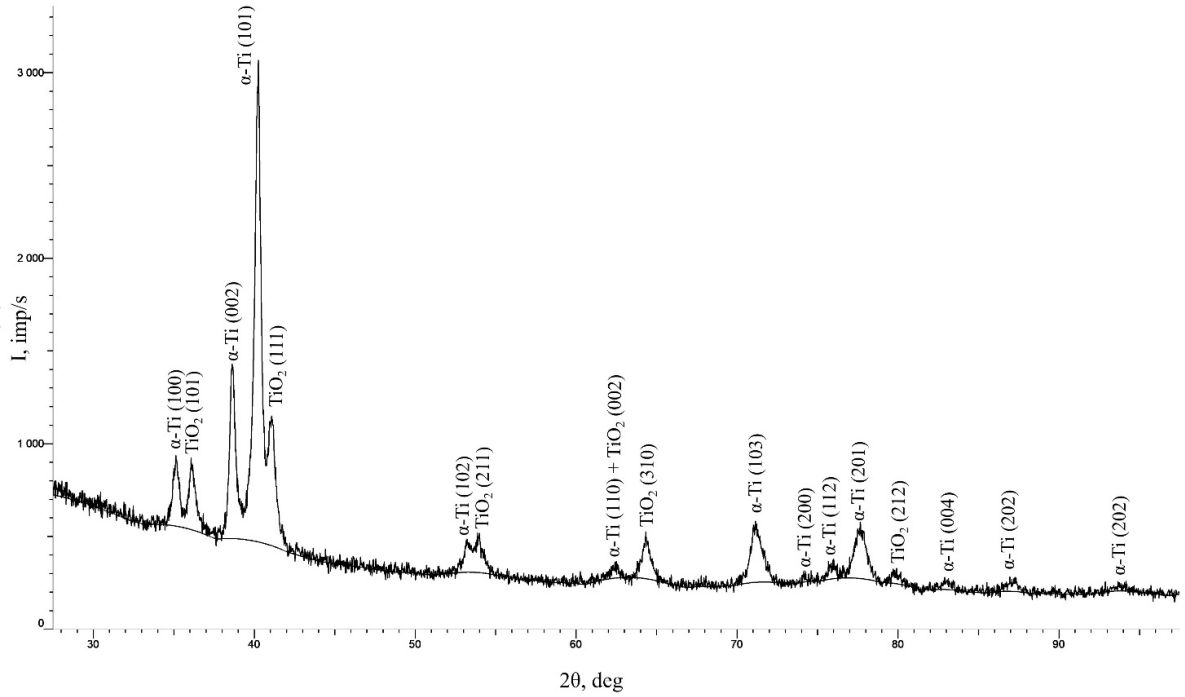

Fig. 1. X-ray diffraction pattern of the initial powder

Table 2

***LENS* modes**

Powder feed rate	10 g/min
Ar gas supply	coaxial – 10 l/min transport – 3.5 l/min shield – 20 l/min
Nozzle height above surface	9 mm
Laser spot diameter	1,800 μm
Laser power	700…1.300 W, step 100 W
Scanning speed	600…1.000 mm/min, step 200 mm/min

The evaluation of the quality of a single laser track was conducted according to the following criteria:
– the track shape coefficient *f*

$$f = \frac{h}{L},$$

where ***h*** is the height of the track above the substrate; ***L*** is the width of the track (Fig. 2);

– melting coefficient *d*

$$d = \frac{S_p}{S_p + S_h},$$

where S_p and S_h are the areas of the track below and above the substrate surface;

– track width *L*;

– angle at the base of the track θ [15, 16–19].

The acceptable values of these characteristics are provided in Table 3. Additionally, the absence of cracks is one of the important criteria.

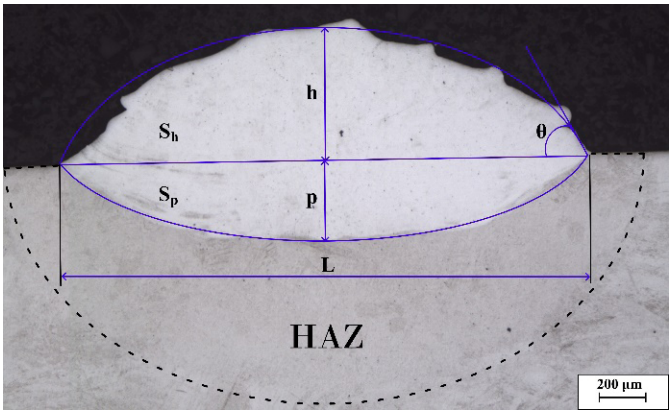

Fig. 2. Shape of the track formed by a laser power of 1.000 W and laser scanning speed of 1.000 mm/min

Table 3

Geometric parameters of a single laser track evaluation criteria

Parameter	Valid value
Shape factor (*f*)	0.2…0.33
Penetration ratio (*d*)	0.1…0.4
Track width (*L*)	1.7…3.0 mm
Angle at the base (θ)	< 90°

During the formation of monolayers, the distance between adjacent tracks varied in the range from 0.5***L*** to 0.9***L***, where ***L*** is the width of the track determined in the previous step. The requirements for the geometric parameters of the mono-layers were as follows: the height variation of the mono-layer should not exceed 30 % of its maximum height, and the depth of melting should be less than 2/3 of the layer height.

For volumetric specimens manufactured under different technological modes, the presence of cracks and large (more than 1–2 µm) pores in longitudinal and transverse sections was monitored.

The microstructure of the manufactured specimens was investigated using an inverted metallographic microscope *Olympus GX-51*. For optical metallography, the specimens were embedded in resin using an automatic press *Struers CitoPress-20* and prepared on a grinding-polishing station *Struers Tegramin 25*. Chemical etching in a aqueous solution of hydrofluoric and nitric acids was used to reveal the structure: 3 ml *HF*, 15 ml HNO_3, 82 ml H_2O.

The microhardness of the specimens was evaluated using the *Vickers* method on a microhardness tester *Pruftechnik KB50 SR*. The indentation load was 1.9 N (200 g), with a measurement error of no more than 10 %.

X-ray diffraction analysis was conducted in the *Bruker D8 Advance* diffractometer with *Bragg-Brentano* focusing scheme in *Cu Kα* radiation in the range of diffraction angles 2θ = 30°–100° with a step of Δ2θ = 0.07° and exposure time of 2 seconds per point. The tube voltage was 40 kV, and the tube current was 35 mA. A semiconductor multichannel detector was used, with a 2 mm slit and *Soller* slit installed on the tube, and only a *Soller* slit on the detector. During the data collection, the specimens were rotated at a speed of 60 rpm. The spectrum processing was conducted using *Diffrac.Eva* and *Diffrac.Topas* software. For X-ray phase analysis, the specimens were electropolished on a *Struers LectroPol-5* in *A2* electrolyte (78 mL $HClO_4$, 90 mL distilled water, 730 mL C_2H_6O, 100 mL $C_6H_{14}O_2$) for 15 min at 10 V.

Results and discussion

According to metallographic analysis, the tracks obtained under all experimental modes (Table 2) are free from cracks, exhibit minimal porosity, and have defect-free boundaries with the substrate material (Fig. 2). A heat affected zone (*HAZ*) with a width of approximately 0.50 ± 0.05 mm is observed at the track boundary.

Analysis the dependence of the track shape coefficient *f* on power revealed that at a scanning speed of 600 mm/min, the coefficient *f* exceeds the permissible range (Figure 3). The geometric parameters of the track obtained at scanning speeds of 800 and 1.00 mm/min meet the requirements for the shape coefficient, bead width, and melting coefficient of the track. The angle at the base of the track is less than 90 degrees for almost all experimental laser deposition modes.

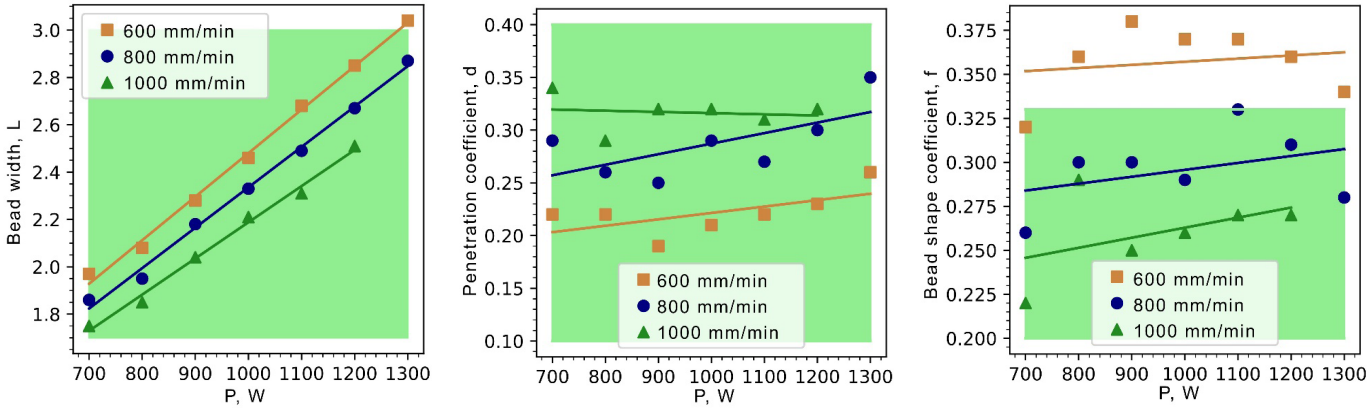

Fig. 3. Dependences of the track width (*a*), penetration ratio (*b*), track shape factor (*c*) on the laser power (green area – range of accepted values)

Microhardness of the tracks manufactured under different modes varies in the range from 386 to 499 HV (Fig. 4). From the graphs, it is evident that increasing the laser power ***P*** results in an increase in hardness, while increasing the scanning speed also results in hardness growth, although this effect is minor. It is known that during the *LENS* process, the material cooling rate is relatively high, which may lead to the formation of a dispersed (α + β) structure and the martensite formation. It can be assumed that the increase in hardness at high laser power is associated with an increase in the temperature gradient.

Based on the track analysis, seven *LENS* modes were selected (Table 4).

The structures of the grown monolayers are presented in Figure 5. A compliance assessment of the monolayers with the specified criteria is shown in the graphs in Figure 6. The manufacturing mode with a distance of 0.9***L*** between adjacent tracks is considered impractical as height variation in some modes is close to 90 %. These specimens consisted not of monolithic layers but of a set of individual tracks. Specimens with a track spacing of 0.5***L*** and 0.7***L*** have approximately the same geometry. The height variation in both cases differs slightly and ranges from 10 to 20 %. It should be noted that at a spacing of 0.5***L***, the layer height was smaller for all *LENS* modes compared to 0.7***L*** (Fig. 6, *b*). This is likely due to the

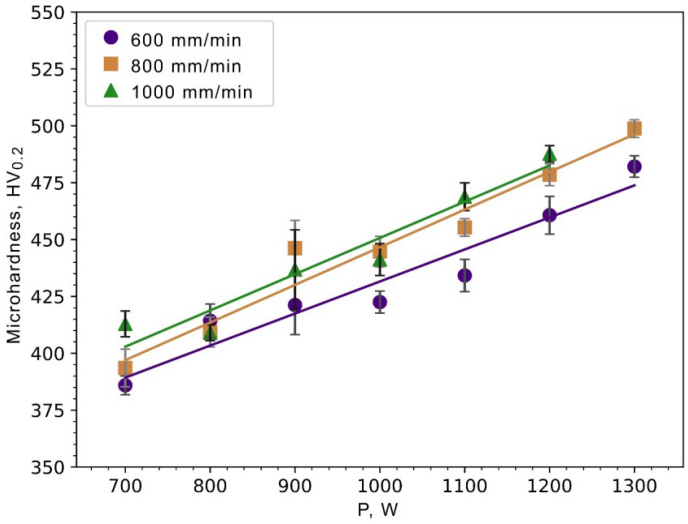

Fig. 4. Dependence of microhardness of single tracks on laser power for different scanning speeds

Table 4

Laser deposition modes selected according to the shape of a single track

Scanning speed ***V***, mm/min	700	800	900	1.000	1.100	1.200	1.300
Laser power ***P***, W	800	1.000	1.000	1.000	1.000	1.000	800

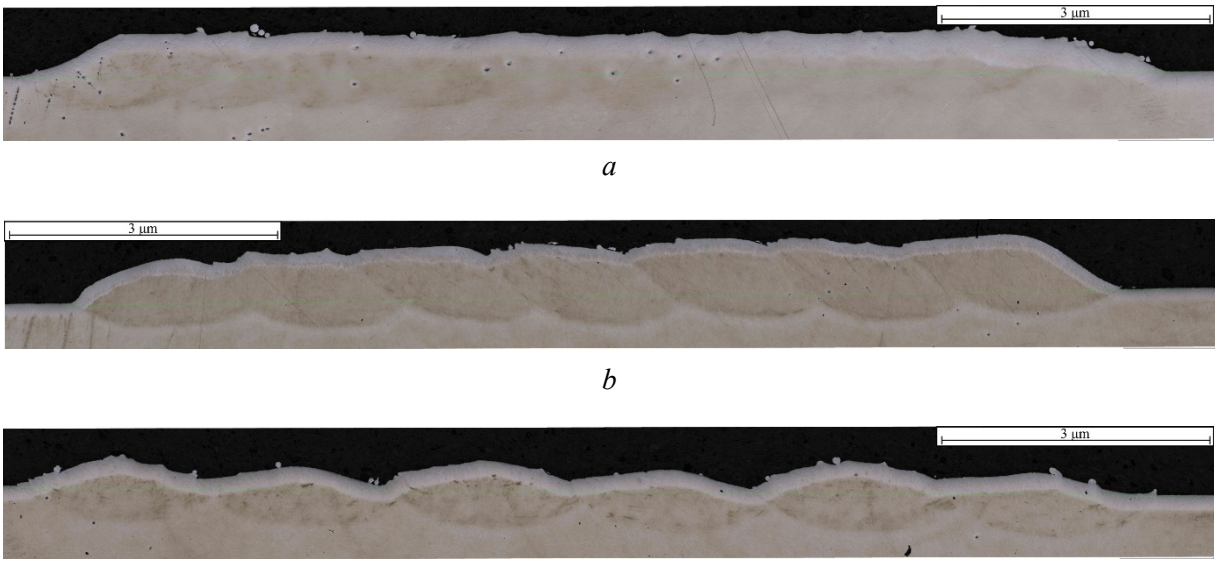

a

b

c

Fig. 5. Structure of monolayers obtained by the *LENS* method with a scanning speed of 1.000 mm/min, power of 1.000 W and different distances between tracks: *a* – 0.5***L***; *b* – 0.7***L***; *c* – 0.9***L***

fact that with a track spacing of 0.5***L***, the forming molten pool captures more material from the neighboring solidified track, which may lead to an increase in the proportion of dispersed powder on it. In other words, these dependencies indicate that the powder material is absorbed to a greater extent with a track spacing of 0.7***L***. It is also worth noting that when the laser power exceeds 1.000 W at a scanning speed of 1.000 mm/min, an increase in the porosity of the monolayers is observed.

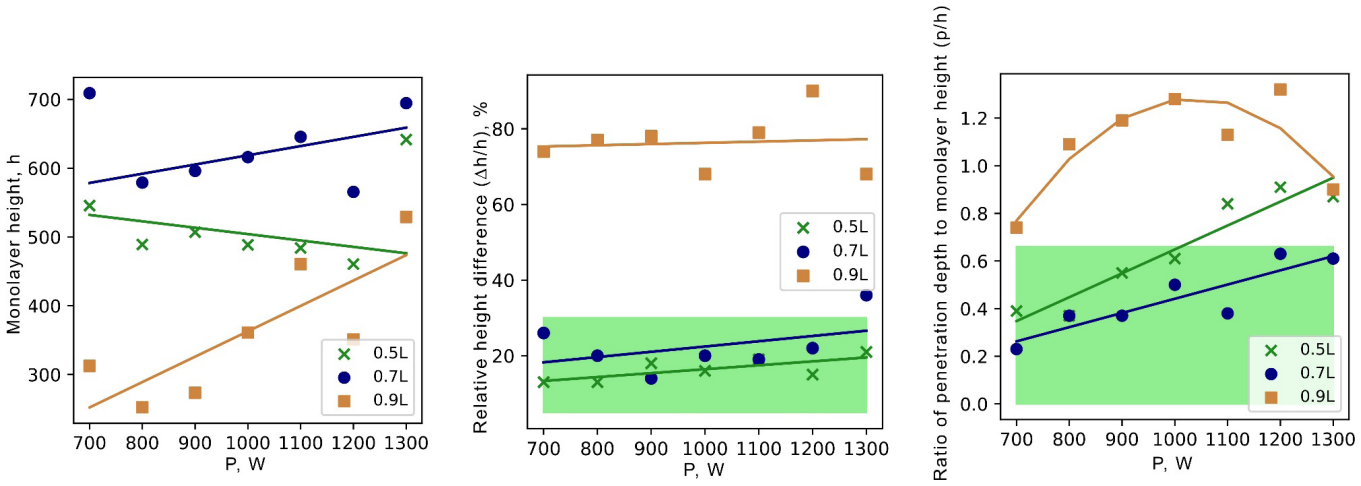

a *b* *c*

Fig. 6. Effect of the distance between tracks on the relative height difference (**Δ*h*/*h***) (*a*), monolayer height (***h***) (*b*), ratio of penetration depth to monolayer height (***p*/*h***) depending on laser power (*c*) (green area – area of acceptable values)

The monolayers microhardness is slightly higher than the one of the previously obtained tracks and amounts to 487 ± 15 HV, while the microhardness value of the monolayer does not depend on the deposition mode (Fig. 7). This result is likely due to the fact that during the laser deposition of multiple tracks, due to the re-heating of the already surfaced material, aging processes occur, i.e., the breakdown of supersaturated solid solutions, resulting in an increase of alloy microhardness.

The modes providing the most uniform layer and the absence of macrodefects were selected to create bulk specimens (Table 5).

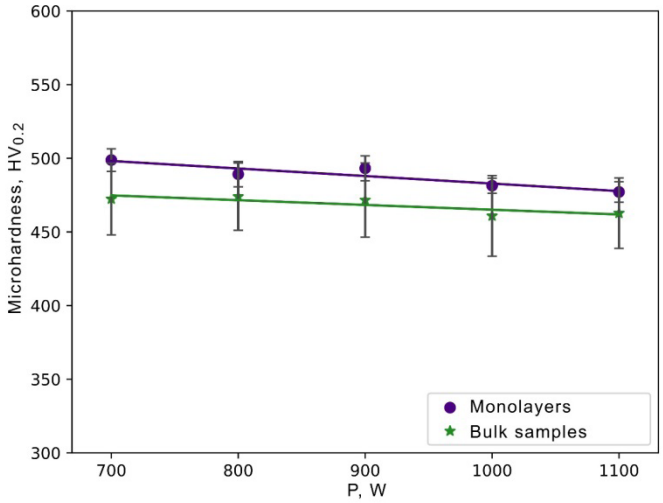

Fig. 7. Dependence of microhardness of monolayers and bulk specimens on laser power

Table 5

Modes selected according to the structure of monolayers

Laser power ***P***, W	700	700	800	800	900	1.000	1.100
Scanning speed ***V***, mm/min	800	800	1.000	1.000	1.000	1.000	1.000
Distance between tracks	0.5***L***	0.7***L***	0.5***L***	0.7***L***	0.7***L***	0.7***L***	0.7***L***

The study of the microstructure of the obtained bulk specimens allows us to conclude that there are no macro-defects. After *LENS* at a laser power of 1,000 W, the α-phase is observed in the form of areas of the so-called "basket weave" and areas of a mesh around primary β-grains (Fig. 8). Such structures are characteristic of this alloy both in the quenched state and after *LENS* [20–23]. Large (~ 100 μm) equiaxed regions of primary β-phase crystals are observed in the scanning plane. Similar structures were observed at other *LENS* modes as well.

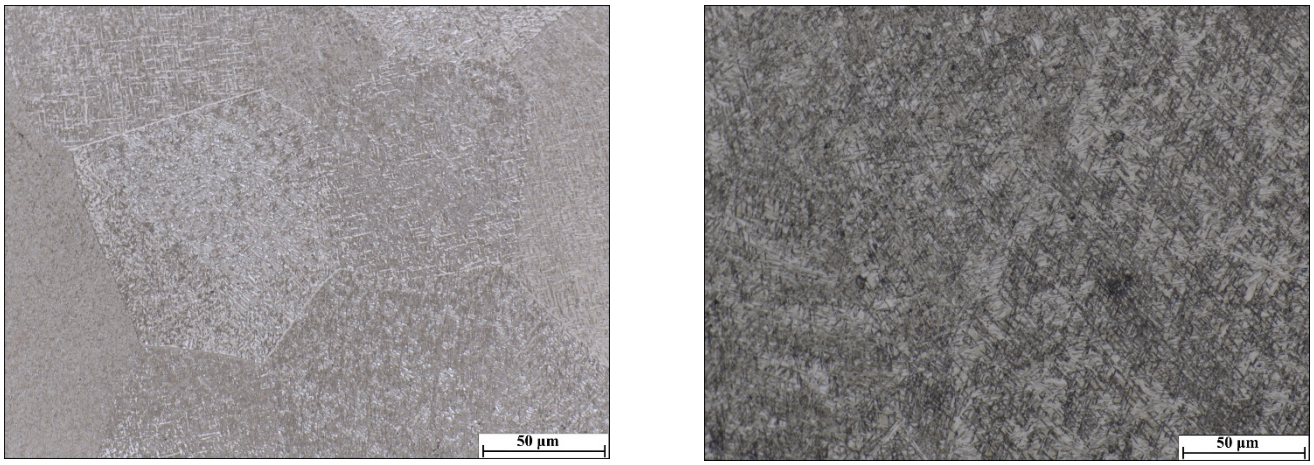

a *b*

Fig. 8. Microstructure of *VT23* alloy after *LENS* (***P*** = 1,000 W; track distance 0.7***L***):
a – laser scanning plane; *b* – cross section of the specimen

When analyzing the dependence of the microhardness of bulk specimens on the deposition mode, it was found that the hardness level at all modes is approximately the same, measuring 457 ± 23 HV (Fig. 7).

Figure 9 presents the results of X-ray phase analysis. All specimens obtained by *LENS* modes exhibit (α + β) phase composition, where α and β are phases with *BCC* and *FCC* crystal lattices, respectively. Since the diffraction peaks of α'-martensite coincide with the peaks of the α-phase, it is not possible to definitively determine its presence in the structure based on the diffraction pattern. It is found that the amount of β-phase constitutes approximately 30 %.

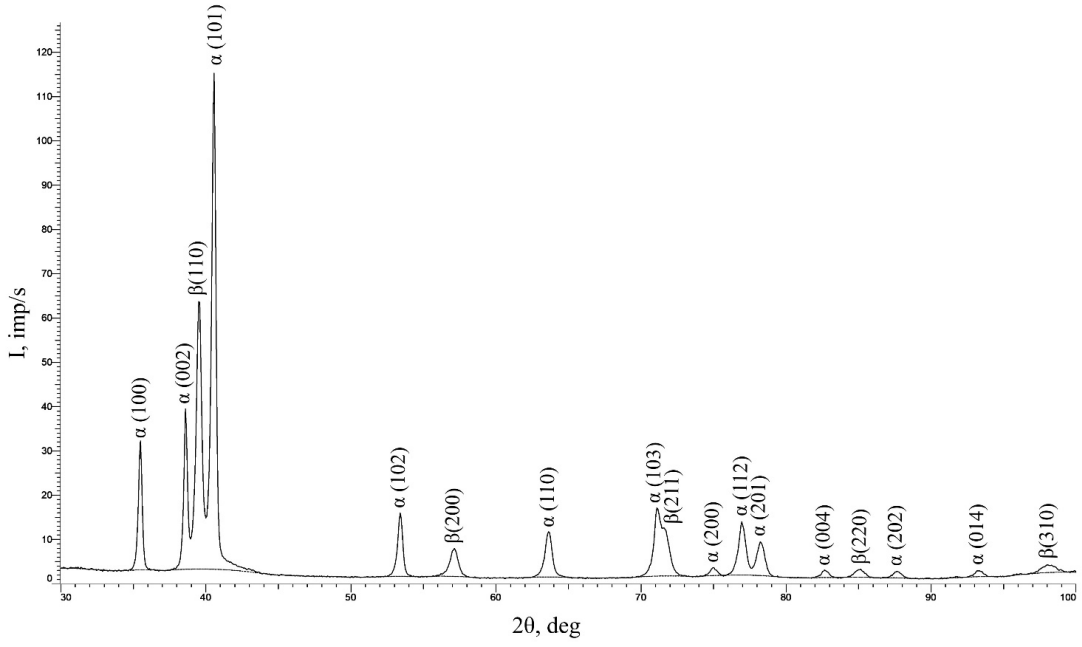

Fig. 9. X-ray diffraction pattern of a bulk specimen at ***P*** = 700 W and 0.5***L***

Conclusion

1. The determination of the *LENS* modes of *VT23* alloy is conducted, allowing the synthesis of objects without cracks, with minimal both porosity and surface roughness, with the specified level of fusion coefficient: laser power P = 700…1.100 W; scanning speed v = 800…1,000 mm/min; the distance between tracks is 0.5…0.7 of the width of the track.

2. Optical metallography revealed that after all experimental *LENS* modes, the structure of the titanium alloy resemble a "basket weave" pattern with dispersed α- and β-phase needle-shaped grains.

3. According to X-ray phase analysis, phase composition of *VT23* alloy doesn't depend on modes and consists of 70 % α-phase and 30 % β-phase.

4. Durometric analysis showed that increasing the laser power results in the microhardness increase of the individual tracks: for a scanning speed of 800 mm/min, increasing the power from 700 to 1.300 W results in the hardness increasing from 390 to 500 HV. However, the increase in power practically does not affect the hardness of monolayers and bulk specimens, maintaining it at an average level of 460 HV.

References

1. Belov S.P., Brun M.Ya., Glazunov S.G., Kolachev B.A. *Metallovedenie titana i ego splavov* [Metallurgy of titanium and its alloys]. Moscow, Metallurgiya Publ., 1992. 352 p.

2. Liu Z., He B., Lyu T., Zou Y. A review on additive manufacturing of titanium alloys for aerospace applications: Directed energy deposition and beyond Ti-6Al-4V. *Jom*, 2021, vol. 73, pp. 1804–1818. DOI: 10.1007/s11837-021-04670-6.

3. Dang L., He X., Tang D., Wu B., Li Y. A fatigue life posterior analysis approach for laser-directed energy deposition Ti-6Al-4V alloy based on pore-induced failures by kernel ridge. *Engineering Fracture Mechanics*, 2023, vol. 289, p. 109433. DOI: 10.1016/j.engfracmech.2023.109433.

4. Ronzhin D.A., Grigoryants A.G., Kholopov A.A. Vliyanie tekhnologicheskikh parametrov na strukturu metalla izdelii, poluchennykh metodom pryamogo lazernogo vyrashchivaniya iz titanovogo poroshka VT6 [Effect of operational parameters on metal structure in products manufactured by direct laser deposition from VT6 titanium powder]. *Izvestiya vysshikh uchebnykh zavedenii. Mashinostroenie = BMSTU Journal of Mechanical Engineering*, 2022, no. 9 (750), pp. 30–42.

5. Ravi G.A., Qiu C., Attallah M.M. Microstructural control in a Ti-based alloy by changing laser processing mode and power during direct laser deposition. *Materials Letters*, 2016, vol. 179, pp. 104–108. DOI: 10.1016/j.matlet.2016.05.038.

6. Mahamood R.M., Akinlabi E.T. Laser power and powder flow rate influence on the metallurgy and microhardness of laser metal deposited titanium alloy. *Materials Today: Proceedings*, 2017, vol. 4 (2), pp. 3678–3684.

7. Safarova D.E., Lugovoi M.E., Ponkratova Yu.Yu., Bazaleeva K.O. [Development of a direct laser growth mode for titanium alloy VT23]. *VIII Vserossiiskaya konferentsiya po nanomaterialam «NANO 2023»* [Proceedings of the VIII All-Russian Conference on Nanomaterials "NANO 2023"]. Moscow, 2023, pp. 242–243. (In Russian).

8. Paydas H., Mertens A., Carrus R., Lecomte-Beckers J., Tchuindjang J.T. Laser cladding as repair technology for Ti–6Al–4V alloy: Influence of building strategy on microstructure and hardness. *Materials & Design*, 2015, vol. 85, pp. 497–510. DOI: 10.1016/j.matdes.2015.07.035.

9. Fatoba O.S., Akinlabi E.T., Akinlabi S.A., Erinosho M.F. Influence of process parameters on the mechanical properties of laser deposited Ti-6Al-4V alloy. Taguchi and response surface model approach. *Materials Today: Proceedings*, 2018, vol. 5 (9), pp. 19181–19190. DOI: 10.1016/j.matpr.2018.06.273.

10. Song L., Xiao H., Ye J., Li S. Direct laser cladding of layer-band-free ultrafine Ti6Al4V alloy. *Surface and Coatings Technology*, 2016, vol. 307, pp. 761–771. DOI: 10.1016/j.surfcoat.2016.10.007.

11. Sinclair L., Clark S.J., Chen Y., Marussi S., Shah S., Magdysyuk O.V., Lee P.D. Sinter formation during directed energy deposition of titanium alloy powders. *International Journal of Machine Tools and Manufacture*, 2022, vol. 176, p. 103887. DOI: 10.1016/j.ijmachtools.2022.103887.

12. Liu Q. Wang Y., Zheng H., Tang K., Li H., Gong S. TC17 titanium alloy laser melting deposition repair process and properties. *Optics & Laser Technology*, 2016, vol. 82. pp. 1–9. DOI: 10.1016/j.optlastec.2016.02.013.

13. Wang T., Zhu Y.Y., Zhang S.Q., Tang H.B., Wang H.M. Grain morphology evolution behavior of titanium alloy components during laser melting deposition additive manufacturing. *Journal of Alloys and Compounds*, 2015, vol. 632, pp. 505–513. DOI: 10.1016/j.jallcom.2015.01.256.

14. Grigor'yants A.G., Misyurov A.I., Tretyakov R.S. Analiz vliyaniya parametrov koaksial'noi lazernoi naplavki na formirovanie valikov [Analysis of the coaxial laser surface coating condition influence on the bead formation]. *Tekhnologiya mashinostroeniya*, 2011, no. 11, pp. 19–21. (In Russian).

15. OST 1-90013–81. *Industry standard. Titanium alloys. Stamps*. Moscow, VIAM Publ., 1981. 7 p. (In Russian).

16. Gibson I., Rosen D., Stucker B., Khorasani M. *Additive manufacturing technologies*. 3rd ed. Cham, Switzerland, Springer, 2021. DOI: 10.1007/978-3-030-56127-7.

17. Lewandowski J.J., Seifi M. Metal additive manufacturing: a review of mechanical properties. *Annual Review of Materials Research*, 2016, vol. 46, pp. 151–186. DOI: 10.1146/annurev-matsci-070115-032024.

18. De Oliveira U., Ocelik V., De Hosson J.T.M. Analysis of coaxial laser cladding processing conditions. *Surface and Coatings Technology*, 2005, vol. 197 (2–3), pp. 127–136. DOI: 10.1016/j.surfcoat.2004.06.029.

19. Harooni A., Nasiri A.M., Gerlich A.P., Khajepour A., Khalifa A., King J.M. Processing window development for laser cladding of zirconium on zirconium alloy. *Journal of Materials Processing Technology*, 2016, vol. 230, pp. 263–271. DOI: 10.1016/j.jmatprotec.2015.11.028.

20. Gladkovsky S.V, Veselova V.E, Patselov A.M, Khotinov V.A. Vliyanie deformatsionnoi stabil'nosti b-fazy v titanovom splave VT23 na fazovyi sostav, strukturu i mekhanicheskie svoistva pri rastyazhenii i udarnom izgibe [The influence of deformation stability of β-phase in titanium alloy BT23 on the phase composition, microstructure and mechanical properties after tension test and impact test]. *Vestnik Permskogo natsional'nogo issledovatel'skogo politekhnicheskogo universiteta. Mashinostroenie, materialovedenie = Bulletin PNRPU. Mechanical engineering, materials science*, 2019, vol. 21, no. 4, pp. 26–33.

21. Shvecov O.V., Kondratyev S.Yu. Vliyanie rezhimov zakalki i stareniya na ekspluatatsionnye svoistva splava VT23 [Effect of quenching and aging modes on the performance properties of the BT23 alloy]. *Nauchno-tekhnicheskie vedomosti SPbPU. Estestvennye i inzhenernye nauki = St. Petersburg Polytechnic University Journal of Engineering Science and Technology*, 2018, vol. 24, no. 2, pp. 119–133.

22. Wang T., Zhu Y.Y., Zhang S.Q., Tang H.B., Wang H.M. Grain morphology evolution behavior of titanium alloy components during laser melting deposition additive manufacturing. *Journal of Alloys and Compounds*, 2015, vol. 632, pp. 505–513. DOI: 10.1016/j.jallcom.2015.01.256.

23. Zhu Y., Tian X., Li J., Wang H. Microstructure evolution and layer bands of laser melting deposition Ti–6.5Al–3.5Mo–1.5Zr–0.3Si titanium alloy. *Journal of Alloys and Compounds*, 2014, vol. 616, pp. 468–474. DOI: 10.1016/j.jallcom.2014.07.161.

Conflicts of Interest

The authors declare no conflict of interest.